**Aalborg Universitet**



# Improvement of Frequency Regulation in VSG-Based AC Microgrid via Adaptive Virtual Inertia

Hou, Xiaochao; Sun, Yao; Zhang, Xin; Lu, Jinghang; Wang, Peng; Guerrero, J. M.

# Improvement of Frequency Regulation in VSG-Based AC Microgrid via Adaptive Virtual Inertia

Xiaochao Hou, *Student Member, IEEE*, Yao Sun, *Member, IEEE*, Xin Zhang, *Member, IEEE*, Jinghang Lu, *Member, IEEE*, Peng Wang, *Fellow, IEEE*, and Josep M. Guerrero, *Fellow, IEEE*

**[1]*Abstract*—A virtual synchronous generator (VSG) control based on adaptive virtual inertia is proposed to improve dynamic frequency regulation of microgrid. When the system frequency deviates from the nominal steady-state value, the adaptive inertia control can exhibit a large inertia to slow the dynamic process and thus improve frequency nadir. And when the system frequency starts to return, a small inertia is shaped to accelerate system dynamics with a quick transient process. As a result, this flexible inertia property combines the merits of large inertia and small inertia, which contributes to the improvement of dynamic frequency response. The stability of the proposed algorithm is proved by Lyapunov stability theory, and the guidelines on the key control parameters are provided. Finally, both hardware-in-loop (HIL) and experimental results demonstrate the effectiveness of the proposed control algorithm.**

***Index Terms*--AC microgrid, adaptive virtual inertia, frequency stability, virtual synchronous generator (VSG).**

## I. INTRODUCTION

DISTRIBUTED generation (DG) is an attractive option in modern electricity production because of its energy sustainable and environmental friendly [1]. For most DGs, photovoltaic, wind, fuel cells, micro-turbine and storage units are normally connected through power electronic interfaces to form an autonomous microgrid system [2], as shown in Fig. 1. Microgrids can operate in both grid-connected mode and islanded mode [3]. In grid-connected mode, the microgrid voltage/frequency and supply-demand power balance are mainly held by the utility grid. While in the islanded mode, the inverter-based DGs should be responsible for keeping the voltage/frequency stability and maintaining the proper power sharing according to their corresponded ratings [4].

In the last three decades, the droop-concept-based control

laws have become significant solutions in inverter-based microgrids due to the salient features of communication-free and plug-and-play capability [5]-[6]. Conventionally, the active power-frequency ($P$-$\omega$) droop and reactive power-voltage droop ($Q$-$V$) are deployed to generate frequency and voltage reference for an inverter-based DG according to output power commands. Hence, each DG contributes to the regulation of system voltage and frequency [7]. However, due to the lack of rotating kinetic energy like in synchronous generator (SG), the droop-controlled inverter-based microgrid has small inertia, which is detrimental to the dynamic frequency stability [8]. Especially when the penetration of static DG units is gradually increased, it would lead to poor voltage/frequency response and even be prone to instability during large disturbances [9].
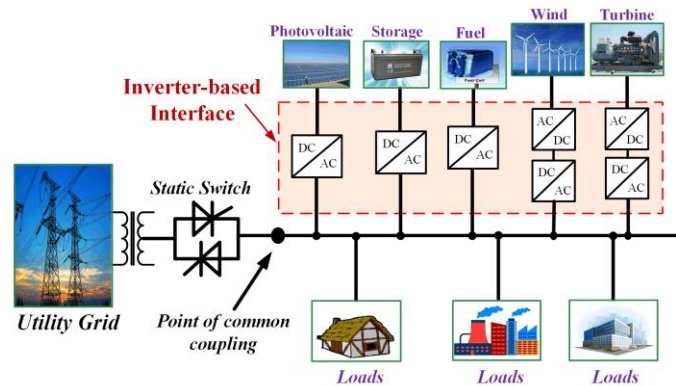


Fig. 1. A general scheme of an inverter-based AC microgrid.

To address this issue, the virtual synchronous generator (VSG) has provided an appropriate solution [10]-[18]. By adding energy storages alongside DGs, the virtual inertia emulation technique is adopted into the photovoltaic system [10]-[11] and full-converter wind turbines [12]-[13]. In 2007, Beck and Hesse [14] conducted the first implementation of VSG. Later, some improved virtual inertia control methods have been proposed to achieve damping power oscillation [15], frequency robustness [16], satisfactory frequency response [17], and power decoupling [18]. In particular, Zhong [19] has built a creative synchronverter for inverter-based DGs. Then, the stability and parameter design of synchronverter are analyzed in grid-connected mode [20] and islanded mode [21]. To obtain a better stability performance of synchronverter, [22] proposed five modifications of virtual inductor, virtual capacitor and anti-windup. Besides, some comparative studies of these control algorithms were described in theoretical reviews [23]-[24].

In order to further explore the benefits of VSG, some recent studies on the adjustable inertia and damping technology [25]-[29] are carried out. As inverter-based DGs are not limited to

physical constraints against SG, the inertia and damping parameters can be flexibly designed in real-time [25]. In [26], Jaber and Toshifumi took a significant step from a fixed virtual inertia to an alternate inertia. Two independent values of inertia moment are chosen by judging the states of the relative angular velocity difference and its change-rate. Although [26] results in a faster and more stable performance, the influence of frequency derivative term is neglected, and there are only two values of inertia. So, the model describes a switching system, which is susceptible to interferences. In [27], the droop gain is modified as a function of frequency derivative term, whose essence is in fact a variable inertia. The frequency deviation is reduced under disturbances. But only frequency derivative term is fully considered, without the direction of frequency deviation. In [28], a fuzzy secondary controller based virtual inertia control scheme is proposed to enhance the voltage/frequency dynamic response of microgrids. However, no theoretical analysis on the fuzzy decision table, which is slightly complicated, is conducted. In [29], the benefits of large inertia and small inertia are comprehensively discussed, and a concept of distributed power system virtual inertia is proposed for grid-connected converters. Despite the effectiveness of controlled virtual inertia methods [25]-[29], they all have to acquire the frequency derivative ($df/dt$) to realize the variable virtual inertia, which is sensitive to measurement noise [30], [31].

To overcome the above disadvantages, we propose an adaptive virtual inertia method to support the frequency stability, as the one in [32], and with new capacities. A large inertia is implemented when the frequency deviates from the nominal value, while a small inertia is adopted to accelerate system dynamics when the frequency returns back the nominal frequency. As the proposed method combines the advantages of both large inertia and small inertia, the improved frequency regulation performance is obtained. Compared to the conventional VSG control methods with variable inertia [25]-[28], the proposed control has three main improvements:

- ***A concise and unified mathematical equation of adaptive virtual inertia***. In [25]-[28], the inertia moment has some scattered small-large values, which is an intuitive and qualitative analysis. Instead, the solution in this study adopts a concise and unified mathematical equation to describe the dynamic of inertia.
- ***A practical control method without derivative action***. In [25]-[28], the inertia moment is given by sampling and determining of frequency derivative ($df/dt$), which may suffer from high-frequency noises. In this study, the proposed algorithm conquers this chattering deficit without frequency derivative action
- ***Strict stability proof and detailed design guidelines***. In this work, the stability of the proposed nonlinear control algorithm is analyzed by Lyapunov stability theory [33], and guidelines for designing key parameters of equivalent swing equation are provided.

The rest of the paper is organized as follows: Section II discusses the analogy between droop control and virtual synchronous generator. The proposed adaptive virtual inertia is presented in Section III. Section IV analyzes the convergence of the control algorithm. Then, the guidelines on the control system design are given in Section V. Hardware-in-loop (HIL) and experimental results are revealed in Sections VI and VII, respectively. Finally, conclusions are given in Section VIII.

## II. ANALOGY BETWEEN DROOP CONTROL AND VIRTUAL SYNCHRONOUS GENERATOR

To facilitate load sharing and improve system reliability, the conventional droop control methods are very popular in parallel inverter systems, as shown in Fig. 2. The frequency and magnitude of the output voltage reference depend on output active power and reactive power, respectively.

$$\omega = \omega^* - \frac{m}{\tau s + 1}(P - P^*) \qquad (1)$$

$$V = V^* - \frac{n}{\tau s + 1}(Q - Q^*) \qquad (2)$$

where $\omega^*$ and $V^*$ indicate the reference values of $\omega$ and $V$ at nominal condition; $P^*$ and $Q^*$ stand for the nominal power references; $\tau$ is the time constant of the low-pass filter (LPF) which filters out the averaged active and reactive powers; $P$ and $Q$ are output active and reactive powers; $m$ and $n$ are the $P$-$\omega$ and $Q$-$V$ droop coefficients, which are chosen as follows:

$$m = \frac{\omega_{\max} - \omega_{\min}}{P_{\max} - P_{\min}}; \quad n = \frac{V_{\max} - V_{\min}}{Q_{\max} - Q_{\min}} \qquad (3)$$

where $\omega_{max}$ and $\omega_{min}$ are the maximum and minimum values of the allowable angular frequency; $V_{max}$ and $V_{min}$ are the maximum and minimum values of the permissible voltage amplitude; $P_{max}$ and $P_{min}$ are the maximum and minimum capacities of the active power; $Q_{max}$ and $Q_{min}$ are maximum and minimum capacities of the reactive power.
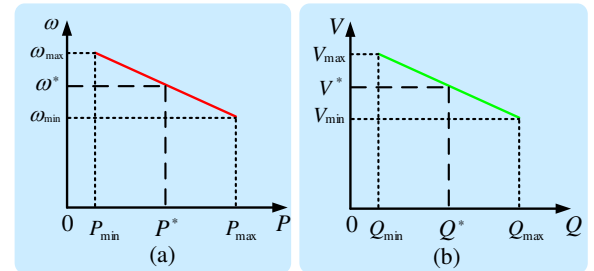


Fig. 2. Conventional droop characteristics for AC microgrid. (a) $P$-$\omega$ droop control. (b) $Q$-$V$ droop control.

Rewrite (1) as follows

$$\frac{\tau}{m}\frac{d(\omega - \omega^*)}{dt} = P^* - P - \frac{1}{m}(\omega - \omega^*) \qquad (4)$$

By comparing (4) with the traditional 2-order swing equation of a SG, the inertia term $J$ and damp term $D$ are equivalent to

$$J = \frac{\tau}{m}; \qquad D_m = \frac{1}{m} \qquad (5)$$

From (4)-(5), the droop control is functionally equivalent to a VSG with a small inertia [34]. Meanwhile, inertia moment depends on the time constant of the LPF.

2
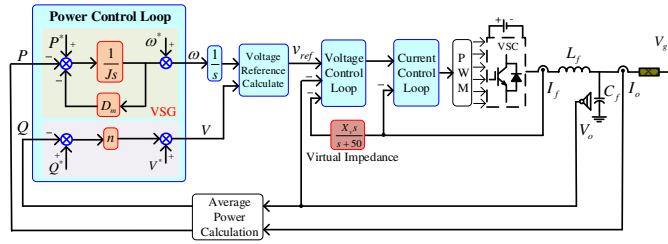
Fig. 3. Typical VSG control diagram of an inverter-based DG.

Fig. 3 presents a typical VSG control scheme of inverter-based DG, which includes a power control loop and dual closed voltage-current loops. The outer power control loop includes an active power control of VSG and a reactive power droop control. A fixed virtual impedance is adopted to decouple *P/Q* and to reduce the impact of the line impedance mismatch [35]. It is implemented by using the high-pass filter instead of a pure derivative operation [35]. Moreover, virtual impedance also has an effect on the system stability, transient response, and power flow performance [36], [37].

## III. PROPOSED ALGORITHM OF ADAPTIVE VIRTUAL INERTIA

### A. Comparison between SG and Droop-based DG

Inertia is a measure of an object's reaction to changes. In conventional SG of power system, the rotor can slowly release rotational kinetic energy (around 10s) when the disturbance occurs, such as, unbalanced supply-demand power. In other words, the SG has a large inertia, which implies a capability of over-load and disturbance rejection. However, for a microgrid, the inverter-based DGs have a fast response speed (about 10ms). If only conventional droop control is adopted in the inverter-based DGs, a small inertia would lead to sharp frequency variation, with load change and source uncertainty. To improve the dynamic frequency regulation, the control strategies of DGs should mimic not only primary frequency control but also the virtual inertia control.

TABLE I.
Potential Advantages/Drawbacks of Large/Small Inertia Based Control

| | Advantages/ Drawbacks |
|---|---|
| Large Inertia (*SG*) | ✓ Decrease the frequency deviation in transient process;<br>✓ Have an over-load capability to some extent. |
| | ✗ Require a high power storage capacity ;<br>✗ Lead to power oscillation easily;<br>✗ Decelerate the dynamic process of frequency returning. |
| Small Inertia (*Droop -based DG*) | ✓ Run quickly to ensure transient load sharing;<br>✓ Accelerate the process of frequency returning. |
| | ✗ Cause big frequency deviation subject to sudden change. |

The potential advantages and drawbacks of large/small inertia based control are discussed in Table I. A relatively large inertia can decrease the frequency deviation in transient process, but the corresponding storage is required and power oscillations is triggered easily. Especially when the system operates with a large frequency deviation, it aggravates the process of frequency returning. On the other hand, system with a small inertia can react quickly to ensure the transient load sharing and ameliorate the frequency returning process, but it may lead to severe frequency deviation when load

demand suddenly changes.

To fully integrate advantages of large inertia and small inertia, this study focuses on two issues: 1) how to design a proper value of inertia moment *J* according to real-time operation states? 2) How to realize the control algorithm for DGs in a practical way to avoid a derivative action?

### B. Proposed Adaptive Virtual Inertia

To address the first issue, an adaptive virtual inertia algorithm is presented in this section. Fig.4 shows the frequency curve deviating from the nominal steady-state value (50Hz) and returning to nominal value under a small disturbance. The nominal steady-state (50/60Hz) is unchanged. As shown in Fig. 4 and Table II, the system should have a slow response when the frequency deviates from the nominal reference, and thus a large inertia should be adopted. On the other hand, a small inertia should be adopted to accelerate system dynamics when the frequency returns back the nominal frequency. To that end, a concise and unified mathematical equation of the adaptive virtual inertia is constructed as follow

$$ J = J_0 + k(\omega - \omega^*)\frac{d\omega}{dt} \qquad (6) $$

From (6), the constructed inertia has two terms. The first term $J_0$ is the nominal constant inertia, and the second term $k(\omega - \omega^*)(d\omega/dt)$ is the adaptive compensation inertia. $k$ is a positive inertia compensation coefficient, which can adjust the response speed of the frequency dynamic. Actually, the total moment of inertia is modified based on the relative angular velocity $(\omega - \omega^*)$ and its change-rate $(d\omega/dt)$ in real-time. Specially, in the nominal steady-state ($\omega = \omega^*$), the second term of adaptive compensation inertia would be 0, and the total inertia is equal to $J_0$.
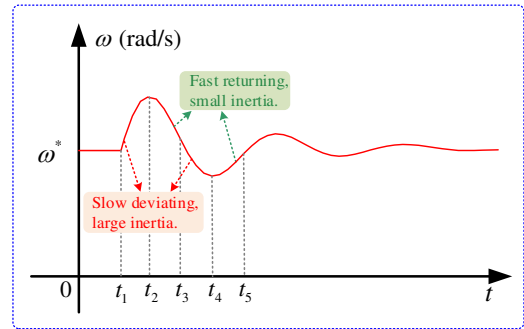


Fig. 4. Adaptive virtual inertia with a large inertia in frequency deviating and a small inertia in frequency returning.

TABLE II.
Design Principles of Virtual Inertia at Different Operation States

| Segment | $\omega_s = \omega - \omega^*$ | $d\omega/dt$ | $\omega$ State | Inertia $J$ |
|---|---|---|---|---|
| $t_1$-$t_2$ | > 0 | > 0 | Deviating | Large value |
| $t_2$-$t_3$ | > 0 | < 0 | Returning | Small value |
| $t_3$-$t_4$ | < 0 | < 0 | Deviating | Large value |
| $t_4$-$t_5$ | < 0 | > 0 | Returning | Small value |

### C. Practical Control Scheme without Derivative Action

In (6), it is worth noting that the adaptive inertia value would be inaccurate if we calculate it directly since the frequency derivative is sensitive to measurement noise [30]-[31]. Thus, we need to find a practical and effective method to

3

address the second issue.

Substituting the constructed inertia (6) into the typical VSG control (4)-(5) yields

$$(J_0 + k\omega_s \frac{d\omega_s}{dt})\frac{d\omega_s}{dt} = P^* - P - D_m\omega_s \quad (7)$$

where $P^*$ is the nominal power reference, and $\omega_s$ represents the slip frequency

$$\omega_s = \omega - \omega^* \quad (8)$$

Rewriting (7) yields

$$k\omega_s(\dot{\omega}_s)^2 + J_0\dot{\omega}_s + D_m\omega_s = P_{rsrv} \quad (9)$$

$$P_{rsrv} = P^* - P \quad (10)$$

where $P$ is the output active power. $P_{rsrv}$ is the reserved power, which implies the difference between nominal power and actual output power.

Obviously, equation (9) is a quadratic equation in the variable $\dot{\omega}_s$. According to the Vieta Theorem, two roots are solved

$$\dot{\omega}_s = \frac{-J_0 \pm \sqrt{J_0^2 - 4k\omega_s(D_m\omega_s - P_{rsrv})}}{2k\omega_s} \quad (11)$$

As both $\omega_s(\dot{\omega}_s) > 0$ and $\omega_s(\dot{\omega}_s) < 0$ may exist in (6), only one root of (11) is effective, derived as follow

$$\dot{\omega}_s = f(\omega_s, P_{rsrv}) = \frac{-J_0 + \sqrt{J_0^2 - 4k\omega_s(D_m\omega_s - P_{rsrv})}}{2k\omega_s} \quad (12)$$

To avoid the singular point ($\omega_s = 0$), rewrite (12) by numerator rationalization

$$\dot{\omega}_s = f(\omega_s, P_{rsrv}) = \frac{-2(D_m\omega_s - P_{rsrv})}{\sqrt{J_0^2 - 4k\omega_s(D\omega_s - P_{rsrv})} + J_0} \quad (13)$$

Then, the improved active power-frequency ($P$-$\omega$) control based on adaptive virtual inertia algorithm is obtained by combining (8) and (13).

$$\omega = \omega^* + \omega_s = \omega^* + \int f(\omega_s, P_{rsrv})dt \quad (14)$$

From (14), the angular frequency reference is a function of output active power. The detailed control scheme with adaptive virtual inertia is presented in Fig. 5. The control input is the real-time active power. The control output is the angular frequency reference. The control function (14) is derived from (6)-(7), and its design principle is shown in Table II. Compared with the power loop of a typical VSG in Fig. 3, the control algorithm with adaptive virtual inertia is added. It is worth noting that only output active power is fed-back in Fig. 5, where the frequency derivative term is avoided. Thus, the proposed control scheme is simple and practical.
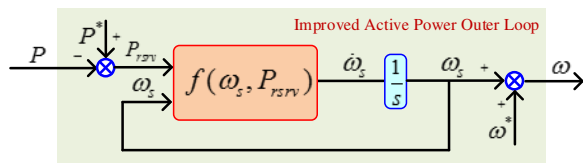


Fig. 5. Improved active power outer loop based on adaptive virtual inertia.

## IV. STABILITY PROOF OF PROPOSED ALGORITHM

### A. Single Inverter-based DG in Grid-Connected Mode

The stability of the proposed control algorithm will be investigated based on Lyapunov stability theorem. The model of a single DG connected to an infinite bus, is firstly built to study the steady and transient states [38] as shown in Fig. 6.
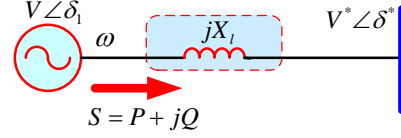


Fig. 6. Equivalent circuit of a DG unit connected to an infinite bus.

Assume that the line impedance is highly inductive [35], and the inverter-based DG is well designed with a salient time-scale separation [48]. Then, the delivered power from a DG to the bus is given by (15).

$$P = \frac{VV^*}{X_l}\sin\delta \quad (15)$$

$$\delta = \delta_1 - \delta^* = \int(\omega - \omega^*)dt \quad (16)$$

where $V$, $\delta_1$ and $\omega$ are the output voltage amplitude, angle and angular frequency of an inverter-based DG; $V^*$, $\delta^*$ and $\omega^*$ are the voltage amplitude, angle and angular frequency of the bus, respectively. $X_l$ is the line reactance, $\delta$ is the power angle.

Combining (9) and the power transmission characteristic (15) yields

$$k\omega_s(\dot{\omega}_s)^2 + J_0\dot{\omega}_s + D_m\omega_s = P^* - \frac{VV^*}{X_l}\sin\delta \quad (17)$$

Rewrite (17) in the form as

$$\begin{cases} \dot{\delta} = \omega - \omega^* = \omega_s \\ \dot{\omega}_s = \frac{1}{J_0}\left(P^* - \frac{VV^*}{X_l}\sin\delta - (D_m + k\dot{\omega}_s^2)\omega_s\right) \end{cases} \quad (18)$$

Note that the term of adaptive virtual inertia can also be regarded as a positive damping $k\dot{\omega}_s^2$ in (18). In the other words, the system damping changes from original $D_m$ to $(D_m + k\dot{\omega}_s^2)$ after using adaptive virtual inertia control.

Then, the state variables $[x_1 \ x_2]^T = [(\delta - \delta_0) \ \omega_s]^T$ are chosen. Rewrite (18) as

$$\begin{cases} \dot{x}_1 = x_2 \\ \dot{x}_2 = a\sin\delta_0 - a\sin(x_1 + \delta_0) - b(D_m + k(\dot{x}_2)^2)x_2 \end{cases} \quad (19)$$

where

$$\begin{cases} \delta_0 = \arcsin\frac{P^* X_l}{VV^*} \\ a = \frac{VV^*}{J_0 X_l} > 0; \quad b = \frac{1}{J_0} > 0 \end{cases} \quad (20)$$

A candidate Lyapunov function is constructed as follows

$$E(x) = \frac{1}{2}(x_2)^2 + a\int_0^{x_1}\left[\sin(x_1 + \delta_0) - \sin\delta_0\right]dx_1 \quad (21)$$

Equation (21) is positive definite under the condition that

4

$-\pi \le x_1 \le \pi - 2\delta_0$. $\dot{E}(x)$ is obtained as

$$\dot{E}(x) = -b\left(D_m + k(\dot{x}_2)^2\right)(x_2)^2 \le 0 \qquad (22)$$

According to (22) and La Salle's Invariance Principle, we have proved that the proposed control algorithm is convergent under the domain of attraction

$$-\pi + \delta_0 \le \delta \le \pi - \delta_0 \qquad (23)$$

### B. Synchronization of Multiple DGs in Islanded Mode

Multiple inverter-based DGs must synchronize with each other to guarantee the stable operation [39]. The case in islanded mode is different from that in grid-connected mode where an infinite bus is assumed. But, in islanded mode, there is an interaction among DGs, and the common bus is slack, which is determinated by all DGs [36]. Herein, the model of multiple DGs using adaptive virtual inertia is analyzed to verify the frequency synchronization.

As shown in Fig. 7, $V_i$, $\delta_i$ and $\omega_i$ are output voltage amplitude, angle and angular frequency of $i$-th DG, respectively. $Z_0$ and $\theta_0$ is the load impedance amplitude and angle at the public point. $Z_i$ and $\theta_i$ is the line impedance amplitude and angle between $i$-th DG and the public point. According to the power flow calculation, the output real power $P_i$ of $i$-th DG can be obtained as follow
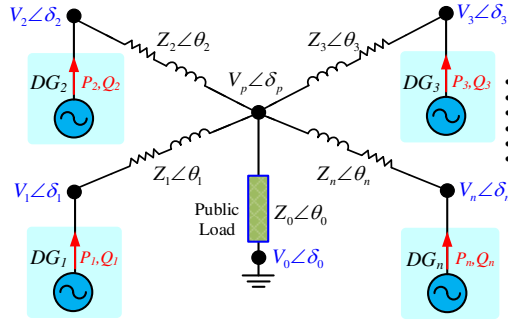


Fig. 7. Schematic of multiple parallel DGs with a public load.

$$P_i = \frac{V_i^2}{|Z_{ii}|}\cos\theta_{ii} - \sum_{j=1, j\neq i}^{n} \frac{V_iV_j}{|Z_{ij}|}\cos(\delta_i - \delta_j + \theta_{ij}) \qquad (24)$$

where

$$\begin{cases} \vec{Z}_{ij} = \vec{Z}_i\vec{Z}_j \sum_{k=0}^{n}(1/\vec{Z}_k); \quad \vec{Z}_{ii} = 1 / \left( \sum_{k=0, k\neq i}^{n}(1/\vec{Z}_{ik}) \right) \\ \theta_{ij} = \arctan\frac{\text{Im}(\vec{Z}_{ij})}{\text{Re}(\vec{Z}_{ij})}; \quad \theta_{ii} = \arctan\frac{\text{Im}(\vec{Z}_{ii})}{\text{Re}(\vec{Z}_{ii})} \end{cases} \qquad (25)$$

Usually, as the line impedance is mainly inductive ($\theta_i \approx \pi/2$) and the load impedance is far greater than the line impedance ($Z_0 \gg Z_i$, $i \in \{1,2...n\}$), (26) can be derived from (25)

$$\theta_{ij} \cong \frac{\pi}{2} \qquad (26)$$

Substituting (26) into (24) yields

$$P_i = k_{ii} + \sum_{j=1, j\neq i}^{n} k_{ij}\sin(\delta_i - \delta_j) \qquad (27)$$

where $k_{ii}$ and $k_{ij}$ are positive coefficients.

$$k_{ii} = \frac{V_i^2}{|Z_{ii}|}\cos\theta_{ii}; \quad k_{ij} = \frac{V_iV_j}{|Z_{ij}|} \qquad (28)$$

As the power angle $\delta_{ij} = \delta_i - \delta_j$ is always small [38], $\sin\delta_{ij} \cong \delta_{ij}$. Then, (27) can be simplified as

$$P_i = k_{ii} + \sum_{j=1, j\neq i}^{n} k_{ij}(\delta_i - \delta_j) \qquad (29)$$

According to (9)-(10), the dynamic of the proposed control algorithm can be accessed for $i$-th DG.

$$k\omega_{si}(\dot{\omega}_{si})^2 + J_0\dot{\omega}_{si} + D_m\omega_{si} = P^* - P_i \qquad (30)$$

where $\omega_{si} = \omega_i - \omega^*$.

Set $\dot{\delta}_{si} = \omega_{si}$, and the dynamic of $i$-th DG is obtained by combining (29) and (30)

$$k\dot{\delta}_{si}(\ddot{\delta}_{si})^2 + J_0\ddot{\delta}_{si} + D_m\dot{\delta}_{si} = P^* - k_{ii} - \sum_{j=1, j\neq i}^{n} k_{ij}(\delta_{si} - \delta_{sj}) \quad (31)$$

where

$$\delta_{si} - \delta_{sj} = \delta_i - \delta^* - (\delta_j - \delta^*) = \delta_i - \delta_j \qquad (32)$$

For a system with $n$ parallel DGs, the system dynamics are presented as follows

$$\begin{cases} g(\dot{\delta}_{s1}, \ddot{\delta}_{s1}) = P^* - k_{11} - \sum_{j=1, j\neq 1}^{n} k_{1j}(\delta_{s1} - \delta_{sj}) \\ g(\dot{\delta}_{s2}, \ddot{\delta}_{s2}) = P^* - k_{22} - \sum_{j=1, j\neq 2}^{n} k_{2j}(\delta_{s2} - \delta_{sj}) \\ \vdots \\ g(\dot{\delta}_{sn}, \ddot{\delta}_{sn}) = P^* - k_{nn} - \sum_{j=1, j\neq n}^{n} k_{nj}(\delta_{sn} - \delta_{sj}) \end{cases} \qquad (33)$$

where

$$g(\dot{\delta}_{si}, \ddot{\delta}_{si}) = k\dot{\delta}_{si}(\ddot{\delta}_{si})^2 + J_0\ddot{\delta}_{si} + D_m\dot{\delta}_{si} \qquad (34)$$

The form of (33)-(34) is subject to the two-way coupling configuration of Van der Pol oscillators [40]-[41]. The convergence of $g(\dot{\delta}_{si}, \ddot{\delta}_{si})$ for a single DG has been proved by (17)-(23) in the Part A of this section. For the coupling multiple DGs, equations (33)-(34) meet the commonly studied update rule of (35) in multi-agent system and nonlinear networked system [42]-[45].

$$\dot{x}_i = -\sum_{j=1}^{n} a_{ij}(x_i - x_j) \qquad (35)$$

As a result, the angles $\delta_{s1}, \delta_{s2}, \cdots, \delta_{sn}$ will converge and synchronize with each other, which means that $\omega_1 = \omega_2 = \cdots = \omega_n$ in steady state [40].

## V. DESIGN GUIDELINES FOR KEY CONTROL PARAMETERS

In this section, the design guidelines for some key control parameters are given, including the droop damping coefficient $D_m$, inertia coefficient $J_0$, and inertia compensation coefficient $k$. Generally, the inertia moment implies a capability of the instant maximum power output. Thus, the inertia coefficient $J_0$ should be designed according to the power capacity of the individual inverter [46]. In addition, the coefficient $D_m$ should

5

be designed by the power sharing among the multiple inverters in the microgrid.

### A. Design Guideline for Droop Damping Coefficient $D_m$

According to the droop characteristic, the system angular frequency should lie in the allowable range $[\omega_{min}, \omega_{max}]$. Thus, the $P$-$\omega$ droop coefficient $m$ in (1)-(3) should meet

$$0 \le m \le \frac{\omega_{\max} - \omega_{\min}}{P_{\max} - P_{\min}} \qquad (36)$$

From (5), that is,

$$D_m = \frac{1}{m} \ge \frac{P_{\max} - P_{\min}}{\omega_{\max} - \omega_{\min}} \qquad (37)$$

Moreover, when choosing $D_m$, a general design guideline should be guaranteed to ensure the power sharing among multiple inverters according to $m_1 P_1^* = m_2 P_2^* = \cdots = m_i P_i^*$ [5].

$$D_{m1} : D_{m2} : \cdots : D_{mi} = P_1^* : P_2^* : \cdots : P_i^* \qquad (38)$$

where $P_i^*$ stands for the rated power capacity of DG-$i$.

### B. Design Guideline for Inertia Coefficient $J_0$

Improper virtual inertia may lead to the power oscillation [34]. So it is necessary to investigate the frequency dynamic in consideration of inertia and damping function together. In the nominal steady-state $(\omega = \omega^*)$, the term of adaptive compensation inertia $k(\omega - \omega^*)(d\omega / dt)$ would be 0, and the total inertia $J$ is equal to $J_0$ in (6). Neglecting the positive damping effect of adaptive compensation inertia $(k=0)$, the dynamic of the nominal steady-state is obtained from (17)

$$J_0 \ddot{\delta} + D_m \dot{\delta} + \frac{VV^*}{X_l} \sin \delta = P^* \qquad (39)$$

Linearization of (39) at the steady-state point yields

$$J_o \Delta\ddot{\delta} + D_m \Delta\dot{\delta} + \frac{VV^* \cos \delta_0}{X_l} \Delta\delta = 0 \qquad (40)$$

For a typical 2nd-order model of (40), the natural frequency $\omega_n$ and damping ratio $\zeta$ are obtained as

$$\omega_n = \sqrt{\frac{VV^* \cos \delta_0}{J_0 X_l}} \; ; \quad \zeta = \frac{D_m}{2} \sqrt{\frac{X_l}{J_0 VV^* \cos \delta_0}} \qquad (41)$$

From (41), the damping ratio of the system depends on the operation points, the values of inertia term $J_0$ and damping term $D_m$. As $\zeta \in [0.1, 1.414]$ should be met to get a satisfactory transient response [38], the inertia coefficient $J_0$ should be chosen as follow:

$$\frac{0.125 D_m^2 X_l}{(V^*)^2} \le J_0 = \frac{D_m^2 X_l}{4\zeta^2 VV^* \cos \delta_0} \le \frac{25 D_m^2 X_l}{(V^*)^2} \qquad (42)$$

### C. Design Guideline for Inertia Compensation Coefficient $k$

In (13), the angular acceleration $\dot{\omega}_s$ must be a real number rather than an imaginary number to ensure the validity of the proposed control. Hence, the following condition must hold identically.

$$J_0^2 - 4k\omega_s(D_m\omega_s - P_{rsrv}) \ge 0 \qquad (43)$$

Especially for two worst cases in Fig. 2,

$$\begin{cases} J_0^2 \ge 4k\omega_s(D_m\omega_s - P_{rsrv}); \; when \; \omega_s = \omega^* - \omega_{\max}; P_{rsrv} = P^* - P_{\min} \\ J_0^2 \ge 4k\omega_s(D_m\omega_s - P_{rsrv}); \; when \; \omega_s = \omega^* - \omega_{\min}; P_{rsrv} = P^* - P_{\max} \end{cases} \qquad (44)$$

In the steady-state as shown in Fig. 2, there exists

$$\begin{cases} P^* - P_{\min} = -D_m(\omega^* - \omega_{\max}) \\ P^* - P_{\max} = -D_m(\omega^* - \omega_{\min}) \end{cases} \qquad (45)$$

Combining (44) and (45) yields

$$J_0^2 \ge \frac{8k(P_{err}^*)^2}{D_m} \qquad (46)$$

where $P_{err}^*$ is the permissible maximum power error

$$P_{err}^* = \max\left\{ P^* - P_{\min}, P_{\max} - P^* \right\} \qquad (47)$$

From (46), the range of the inertia compensation coefficient $k$ is given by

$$0 < k \le \frac{D_m(J_0)^2}{8(P_{err}^*)^2} \qquad (48)$$

In (6), a relatively large value of compensation coefficient $k$ is favorable to exhibit the effectiveness of adaptive inertia control. Thus, $k$ should be chosen as an upper bound from (48).

### D. Parameter Design to Limit Excessive RoCoF

Over-fast returning of frequency may trigger the undesirable rate-of-change-of-frequency (RoCoF) protection relays of generator units [30]. Thus, the local control variable $(\dot{\omega}_s)$ of RoCoF in (12) should be less than the permissible maximum RoCoF value $\dot{\omega}_s^{\max}$.

$$\dot{\omega}_s = \frac{-J_0 + \sqrt{J_0^2 - 4k\omega_s(D_m\omega_s - P_{rsrv})}}{2k\omega_s} < \dot{\omega}_s^{\max} \qquad (49)$$

In (49), $\omega_s \in [\omega^* - \omega_{\max}, \omega^* - \omega_{\min}]$; $P_{rsrv} \in [P^* - P_{\max}, P^* - P_{\min}]$. Considering two worst cases where the load is switched from no-load/full-load to normal-load, the DG frequency would have a fastest returning and the RoCoF would have a maximum value. This is, (49) should hold under the conditions: 1) $\omega_s = \omega^* - \omega_{\max}$; $P = P_{\min} \to P^*$ ; 2) $\omega_s = \omega^* - \omega_{\min}$; $P = P_{\max} \to P^*$. Then, rewriting (49) yields

$$\bar{\omega}_s\left(D_m + k(\dot{\omega}_s^{\max})^2\right) < J_0 \dot{\omega}_s^{\max} \qquad (50)$$

where $\bar{\omega}_s$ is the permissible maximum frequency deviation.

$$\bar{\omega}_s = \max\left\{ \omega^* - \omega_{\min}, \omega_{\max} - \omega^* \right\} \qquad (51)$$

According to (50), the coefficients $D_m$, $J_0$, and $k$ should be synthetically designed to prevent excessive RoCoF levels.

### E. Adaptive Inertia Bound $[J_{min}, J_{max}]$ to Avoid Long-Term Over-Capacity of Converters

Inertia provision is closely related to the available capacity of power sources and inverters [12]. Thus, a bound $[J_{min}, J_{max}]$ of adaptive inertia value is necessary. Then, the parameter constraint is derived from (6)

$$J_{\min} \le J = (J_0 + k\omega_s\dot{\omega}_s) \le J_{\max} \qquad (52)$$

where $J_{max}$ is indicated by the available power capacity of converters [12]. $J_{min}$ is indicated as the minimum value in (46) and (50) to ensure the effectiveness of proposed control algorithm [30].

In order to guarantee the bound in (52), $k$ should also meet (53) by combining (49)-(52).

$$0 \le k \le \min \left\{ \frac{J_0 - J_{min}}{\bar{\omega}_s \dot{\omega}_s^{max}}, \frac{J_{max} - J_0}{\bar{\omega}_s \dot{\omega}_s^{max}} \right\} \qquad (53)$$

## VI. HARDWARE-IN-LOOP (HIL) RESULTS

The proposed adaptive virtual inertia control is verified by real-time HIL tests. As seen in Fig. 8, the HIL system includes

two sections: physical circuits and controller. The physical circuits are realized by the real-time simulator OP5600 whose time-step is 20μs, which can accurately mimic the dynamics of the real-power components. The controller is the real-hardware dSPACE 1202 Microlab-Box, whose sampling frequency is 20 kHZ.
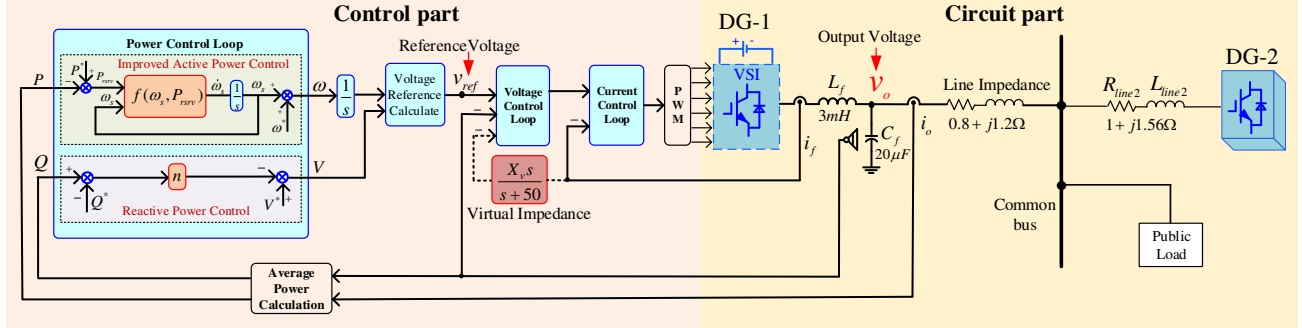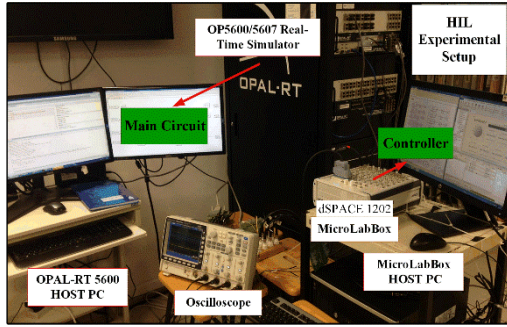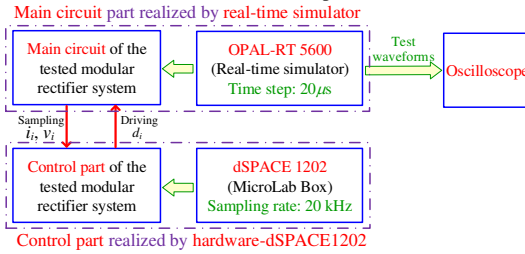


Fig. 9. Schematic diagram of improved power outer loop based on adaptive virtual inertia control algorithm.



(a) Picture of the HIL platform.



(b) Diagram of the HIL platform.
Fig. 8. Hardware-in-loop (HIL) platform.

TABLE III.
HIL Test Parameters

| Parameter | Symbol | Value |
|---|---|---|
| System Parameters | | |
| Nominal frequency | $f^*$ | 50 Hz |
| Nominal voltage | $V^*$ | 311 V |
| Rated active power | $P^*$ | 2 kW |
| Rated reactive power | $Q^*$ | 2 kvar |
| Control Parameters | | |
| Virtual inductance | $X_v$ | 1.8 Ω |
| Power filter time constant | $\tau$ | 1/60 |
| P-$\omega$ droop coefficient | $m$ | 1/600 |
| Q-V droop coefficient | $n$ | 0.01 |
| Droop Damp coefficient | $D_m$ | 600 |
| Small inertia coefficient | $J_0$ | 10 |
| Large inertia coefficient | $J_0$ | 100 |
| Compensation coefficient | $k$ | 0.18 |

Fig.9 shows the model of two parallel DGs. The HIL parameters are listed in Table III. All control parameters of two DGs are identical except different line impedances ($Z_1$=0.8+$j$1.2 Ω; $Z_2$=1+$j$1.56 Ω). The damp coefficient $D_m$ is chosen according to (37)-(38). The small/large inertia coefficients $J_0$ are designed from (42). The inertia compensation coefficient $k$ is calculated by (48). To avoid oscillation, the system is designed to be over-damped.
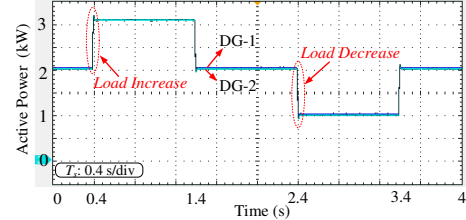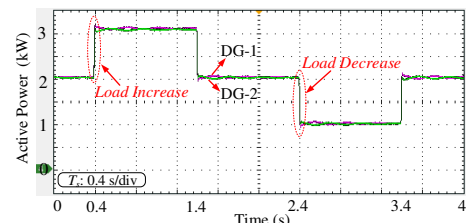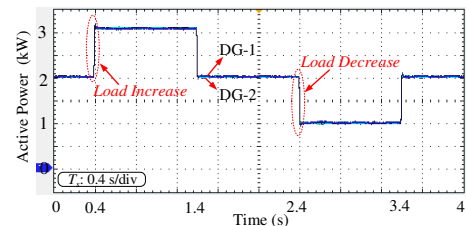


Fig. 10. Output active powers of two DGs under resistive time-varying load. (a) Small inertia ($J_{0\_sml}$=10, $k$=0). (b) Large inertia ($J_{0\_lrg}$=**100**, $k$=0). (c) Adaptive inertia ($J_{0\_adp}$=100, $k$=**0.18**).

### A. Comparisons under Resistive Time-Varying Load

Fig. 10 and Fig. 11 show the HIL results under resistive

time-varying load. To verify the validity of the proposed control, three groups of parameters are applied: (a) small constant inertia $J_{0\_sml}$=10, $k$=0; (b) large constant inertia $J_{0\_lrg}$=100, $k$=0; (c) adaptive inertia $J_{0\_adp}$=100, $k$=0.18. The first case with a small constant inertia represents the conventional droop control from (4)-(5). The second case with a large constant inertia implies the conventional VSG control. The third case with an adaptive inertia represents the proposed control.

Fig. 10 presents the output active power of two DGs. The load demand changes every 1 second. It has an increase in 0.4s and has a decrease in 2.4s with respect to the normal load power 4 kW. As two DGs have the same capacity and same control parameters, the active power responses of three cases are similar in Fig. 10, and the accurate active power sharing is always achieved. Furthermore, it is worth noting that the active power under large constant inertia has a slightly oscillation in Fig.10 (b). However, after adopting the adaptive inertia control, the power oscillation is ameliorated in Fig.10 (c), which reveals that adaptive virtual inertia also has a function of power oscillation damping as shown in (18).
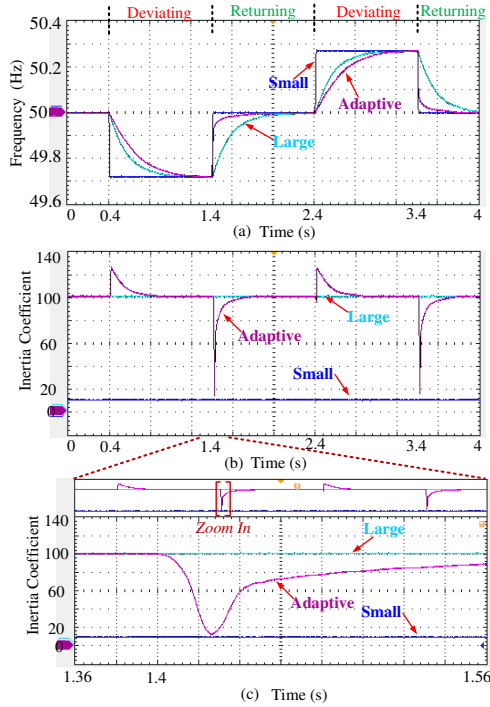


Fig. 11. Comparison of three tests under time-varying load. (a) System frequency. (b) Inertia value of DG-1. (c) Zoomed-in inertia at t∈[1.36s, 1.56s].

Fig. 11 illustrates the comparison of three HIL results under time-varying load. From the frequency response in Fig. 11(a), the deviating time and returning time of three cases are demonstrated in Table IV. In the first case with a small constant inertia control, both the returning time and deviating time are about **0.05**s, which means that the system has a very fast response. In the second case with a large constant inertia, both the returning time and deviating time are about **0.6**s, which reveals that the system has a very slow response. When adopting the proposed control, the system has a shorter returning time **0.2s** and a longer deviating time **0.75s** than that of the large inertia. That is, the system frequency can be

deviated slowly with a relatively large inertia and returned quickly with a relatively small inertia in Fig. 11(b). Moreover, it is noted that both DGs change their inertia simultaneously as they have same control parameters and power rating. Fig. 11(b) just shows the inertia of DG-1 for comparisons. Since the frequency derivative term is not enabled in the proposed control (13)-(14), the inertia regulation exhibits a smooth dynamic process from the thumbnail of Fig. 11(c).

TABLE IV.
Comparison of Three HIL Results

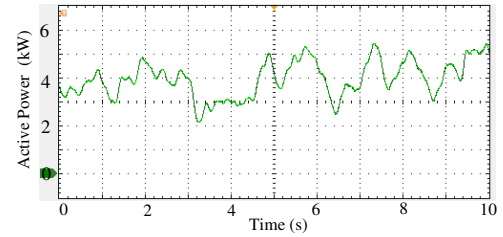| Scenarios | Features | (1) Small inertia | (2) Large inertia | (3) Adaptive inertia |
|---|---|---|---|---|
| **A.** Under time-varying load | $J$ Value | 10 | 100 | [20, 125] |
| | Returning time | 0.05s | 0.6s | **0.2s** |
| | Deviating time | 0.05s | 0.6s | **0.75s** |
| **B.** Under frequent load variation | $J$ Value | 10 | 100 | [20, 125] |
| | Maximum frequency deviation | 0.22 Hz | 0.038 Hz | **0.016** Hz |



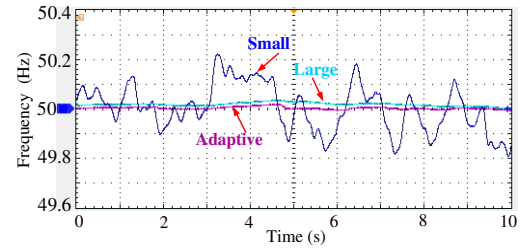Fig. 12. Total load power demand under frequent-variation load.



Fig. 13. Frequency comparison of three tests under frequent-variation load.

### B. Comparisons under Frequent-Variation Load

To further test the performances of the proposed control, three comparative cases are carried out under frequent-variation load. Fig. 12 shows the total power demand of the variable load. Fig. 13 and Table IV discuss the comparison of three HIL results under frequent-variation load. In the first case with a small constant inertia control, the maximum frequency deviation is about 0.22 Hz. In the second case with a large constant inertia control, the maximum frequency deviation is about 0.038 Hz. However, for the adaptive virtual inertia, the maximum frequency deviation is just about 0.016 Hz. As a result, the nominal operation frequency is guaranteed as much as possible under variable loads. Thus, compared with the conventional droop and VSG controls, the proposed method improves the frequency nadir and dynamic response

8

under load variation.

### C. Comparisons under Induction Motor (IM)

In this sub-section, three comparative tests are carried out under the load of squirrel-cage induction motor (IM). The inertia moment of IM is 0.089 kg·m$^2$. The nominal power of IM is 2.2 kW. Fig. 15 shows the total load power when IM is connected to the system at t=0.8s and is switched out at t=2.8s. Before 0.8s, the system operates with a 4kW resistive load. After starting-up the IM load at t=0.8s, a large inrush current is observed in Fig. 14, and the peak value of starting-up stator current is almost twice as large as the nominal current. It is noted that a method of rotor series-resistance is adopted to avoid an over-large current [47].

Fig. 16 shows the frequency performances of three HIL results under IM load. In the first case with a small constant inertia control, the system frequency has a very fast response, and is sensitive to the load oscillation during IM starting-up. In the second case with a large constant inertia, the system frequency has a very slow response in both frequency deviating and returning process. When adopting the proposed adaptive control, the system frequency can be deviated slowly and returned quickly in Fig. 16. As a result, the proposed adaptive inertia control is still effective under IM load.
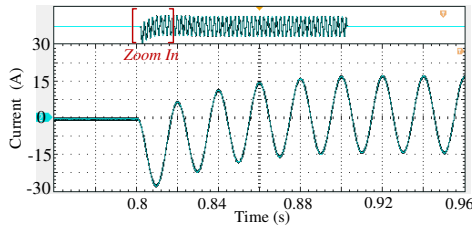


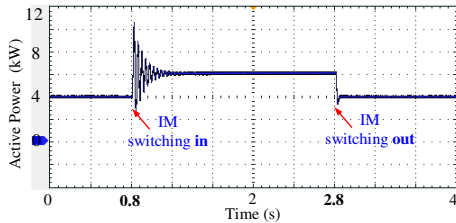Fig. 14. Phase-A stator current of IM at starting-up time.



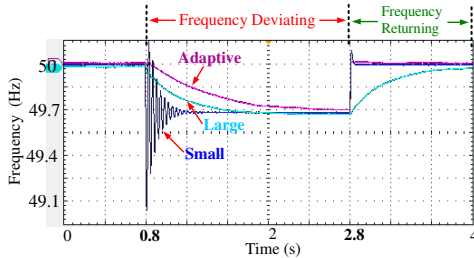Fig. 15. Total load power demand under IM load.



Fig. 16. System frequency comparison of three tests under IM load.

### D. Comparison with alternating inertia method [26]

The purpose of this case is to verify the advantages of proposed control strategy compared with the existing alternating inertia method. In [26], two large/small inertia values are indicated by judging states of the relative angular frequency difference ($\omega_s = \omega - \omega^*$) and its change-rate ($\dot{\omega}_s$). Thus, the method in [26] have to acquire the frequency

derivative (*df/dt*) to realize the alternating inertia. In the contrast test, the basic control parameters are set to the same with the former, such as a small constant inertia $J_{0\_sml}$=10, and a large constant inertia $J_{0\_lrg}$=100.

To test the robustness performances of proposed control, high-frequency noises are imposed into the system operation frequency. The comparison results are shown in Fig. 17. Both two methods have a slow frequency deviating and a fast frequency returning under load changes in Fig. 17(a). Meanwhile, the proposed method has a slightly better performance during two dynamic processes. The main cause of this phenomenon is that the alternating inertia in Fig. 17(b) is sensitive to high-frequency noises. For example, during the frequency deviating process at t∈[0.4s, 1.4s], the alternating inertia is not always a large inertia value due to the inaccurate interference of $\dot{\omega}_s$. Similarly, during the frequency returning process at t∈[1.4s, 2s], the alternating inertia is not always a small inertia value, which has an adverse effect on dynamic response.
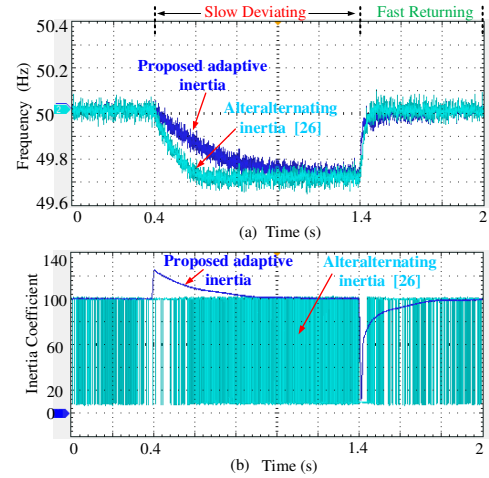


Fig. 17. Comparison with alternating inertia method [26]. (a) System frequency with high-frequency noises. (b) Inertia value of DG-1.
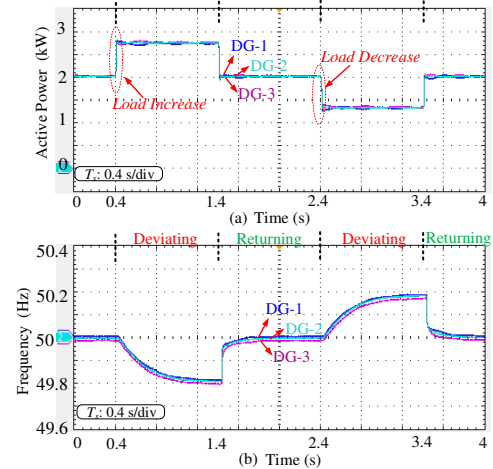


Fig. 18. Results of proposed control with three DGs. (a) Output active powers. (b) Output frequencies.

### E. Proposed Adaptive Inertia Control with Three DGs

Fig. 18 shows the performances of proposed adaptive inertia with three DGs. From Fig. 18(a), the proper active power sharing is achieved among three DGs. Moreover, DGs can

9

synchronize with each other in Fig. 18(b), which verifies the synchronization analysis of multiple DGs in (30)-(35).

### F. Proposed Adaptive Inertia Control with RoCoF Limitation

To validate the practical RoCoF limitation in Section V.D, a permissible maximum RoCoF value 2 Hz/s is set [30], and the coefficient $k$ is changed from 0.18 to 0.08 in this case according to (50). The testing process under resistive time-varying load is same with Section VI.A. The comparison results with/without RoCof limitation are shown in Fig. 19. From the frequency response in Fig. 19 (a), an over-fast frequency returning is be restrained after considering the RoCof limitation. Thus, an undesirable RoCoF protection tripping can be overcome in practical application. Moreover, Fig. 19 (b) reveals that the inertia coefficients have a decreased value under frequency returning and an increased value under frequency deviating, which verifies the effectiveness of adaptive inertia control. Meanwhile, it is clear that the inertia variation range of $k$=0.08 is smaller than that of $k$=0.18. Particularly for frequency returning at $t \in$[1.4s, 2.4s] and $t \in$[3.4s, 4s], an over-small inertia value is prevented to guarantee a lower bound of inertia and limit excessive RoCoF.
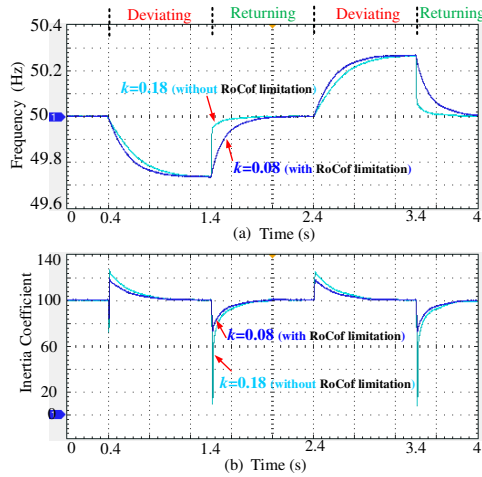


Fig. 19. Comparison results of proposed control with/without RoCoF limitation. (a) System frequency. (b) Inertia value of DG-1.

### TABLE V.
#### Experimental Parameters

| Parameter | Symbol | Value |
|---|---|---|
| System Parameters | | |
| Nominal frequency | $f^*$ | 50 Hz |
| Nominal voltage | $V^*$ | 96 V |
| Rated active power | $P^*$ | 80 W |
| Rated reactive power | $Q^*$ | 80 var |
| Control Parameters | | |
| Virtual inductance | $X_v$ | 1.5 Ω |
| Power filter time constant | $\tau$ | 1/60 |
| $P$-$\omega$ droop coefficient | $m$ | 1/60 |
| $Q$-$V$ droop coefficient | $n$ | 0.01 |
| Droop Damp coefficient | $D_m$ | 60 |
| Small inertia coefficient | $J_0$ | 4 |
| Large inertia coefficient | $J_0$ | 30 |
| Compensation coefficient | $k$ | 1.05 |

## VII. EXPERIMENTAL RESULTS

A prototype shown in Fig. 20 is built to verify the effectiveness of the proposed method. It comprises two DGs based on the single phase voltage source inverters which are controlled by digital signal processors (TMS320f28335) and the sampling rate is 12.8 kHz. The rated system voltage is 96 V/ 50 Hz. The rated power of each DG is 80 W/ 80 var. The experimental parameters are listed in Table V. All control parameters of two DGs are identical.

To verify the proposed control, three groups of parameters are tested: (a) small constant inertia $J_{0\_sml}$=4, $k$=0; (b) large constant inertia $J_{0\_lrg}$=30, $k$=0; (c) proposed adaptive inertia $J_{0\_adp}$=30, $k$=1.05. The voltage and current waveforms of three tests under time-varying load are shown in Fig. 21. The upper zoomed-out windows of three figures in Fig. 21(a)-(c) shows the same load-switching process. The lower zoomed-in windows of three figures in Fig. 21 have three different time instants in order to present the more details of dynamic current performance under different load switching transition. For instance, the details of Fig. 21(a) illustrate the voltage/current waveforms under the load switching from heavy-load to normal-load. Meanwhile, Fig. 21(b) shows the voltage/current waveforms when the load is switched from no-load to normal-load. Finally, Fig.21(c) shows the voltage/current waveforms from normal-load to heavy-load.
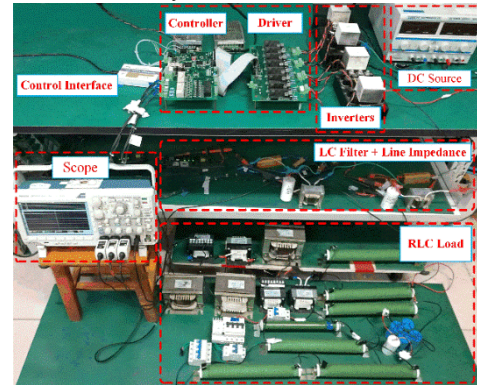


Fig. 20. Experimental prototype of parallel inverters system setup.

In each test, the waveforms from top to down are the output voltage ($U_1$) of inverter 1, the output voltage ($U_2$) of inverter 2, the output current ($I_1$) of inverter 1 and the output current ($I_2$) of inverter 2, respectively. According to Fig. 14, the output active power of experimental results are calculated as shown in Fig. 22. Although the control parameters are different under three cases, the power responses are similar because two DGs are mostly the same. In the other words, the proposed control does not affect the power dynamic response and the power sharing accuracy of the steady-state.

Fig. 23 and Table VI describes the comparison of three experimental results under time-varying load. In the first case with a small constant inertia control, both the returning time and deviating time are about 0.1s with a fast response. In the second case with a large constant inertia control, both the returning time and deviating time are about 2.5s, and a relatively slow response is attained.
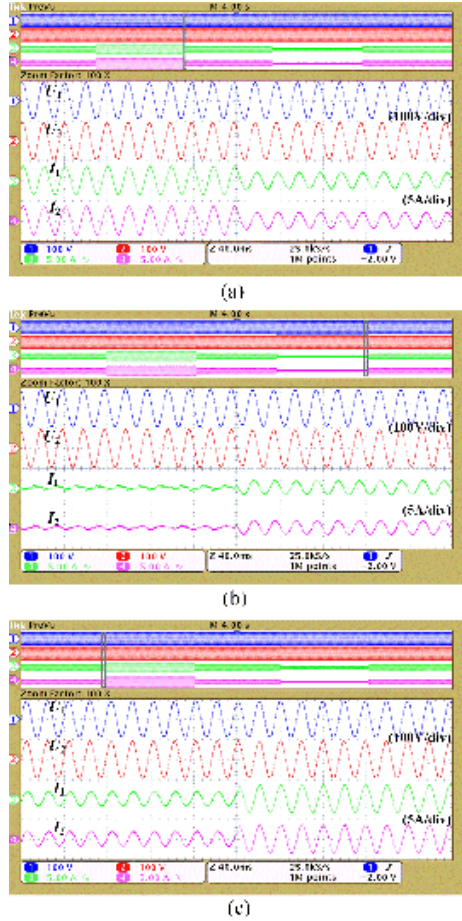
10

Fig. 23. Comparison of three experimental results under time-varying load. (a) System frequency. (b) Inertia value of DG-1.

TABLE VI.
Comparison of Three Experimental Results

| Scenarios | Features | (1) Small inertia | (2) Large inertia | (3) Adaptive inertia |
|---|---|---|---|---|
| Under time-varying load | $J$ Value | 4 | 30 | [6, 37] |
| | Returning time | 0.1s | 2.5s | **0.5s** |
| | Deviating time | 0.1s | 2.5s | **3.5s** |



Fig. 21. Voltage/current waveforms of three tests under same time-varying load. (a) Small inertia ($J_{0\_sml}$=4, $k$=0). (b) Large inertia (**$J_{0\_lrg}$=30**, $k$=0). (c) Adaptive inertia ($J_{0\_adp}$=30, **$k$=1.05**).
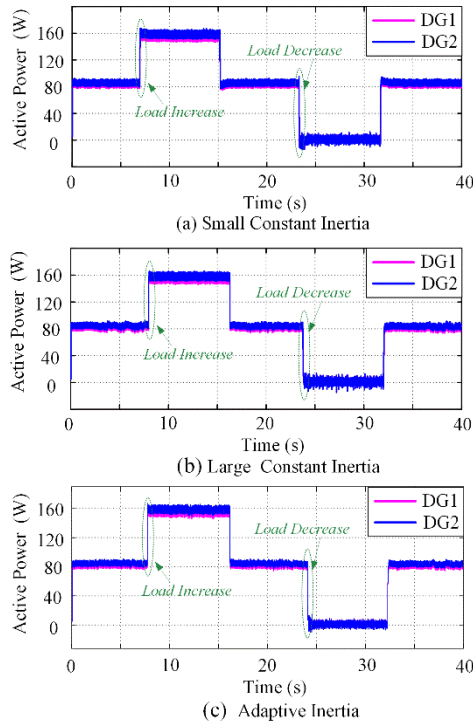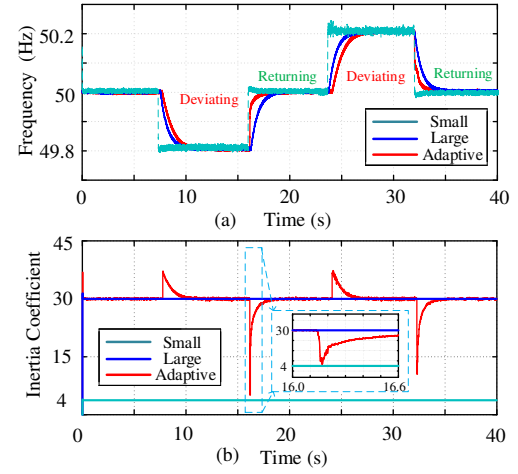


Fig. 22. Active power of experimental result under time-varying load. (a) Small inertia ($J_{0\_sml}$=4, $k$=0). (b) Large inertia (**$J_{0\_lrg}$=30**, $k$=0). (c) Adaptive inertia ($J_{0\_adp}$=30, **$k$=1.05**).

While for the proposed adaptive inertia control, the system has a shorter returning time 0.5s and a longer deviating time 3.5s than that of the large inertia. That is, the system frequency can be deviated slowly with a relatively large inertia and returned quickly with a relatively small inertia in Fig. 23(b). Furthermore, it is noted that both DGs change their inertia simultaneously as they have same control parameters and power rating. Fig. 23(b) just shows the inertia of DG-1 for three experiment comparisons. Since the direct frequency derivative term of (6) is not used in the final proposed control scheme (13)-(14), the smooth inertia dynamic is enabled in Fig. 23(b). Thus, some high-frequency interferences can be avoided, and the control algorithm is practical and robust.

## VIII. CONCLUSION

This study introduces an adaptive virtual inertia control algorithm to improve dynamic frequency regulation of VSG-based microgrids. The advantages of the proposed control algorithm include: 1) a concise and unified mathematical equation of the adaptive virtual inertia is constructed, and 2) a practical control algorithm is proposed to avoid the direct frequency derivative action. Under certain power disturbances, the proposed control has the advantages of both large inertia and small inertia. When the system frequency is deviating away from the nominal value, a large inertia is performed to slow the dynamic process and improve frequency nadir. When the frequency is returning to the nominal value, a small inertia is shaped to quickly accelerate system dynamics. Thus, the frequency regulation performance is greatly improved. The

11

effectiveness of the proposed control is verified under three load types, including resistive time-varying load, frequent-variation load, and induction motor load. On the whole, the proposed method supports frequency dynamics and promotes high penetrations of distributed generations.

## IX. REFERENCES

[1] X. Hou, Y. Sun, H. Han, Z. Liu, W. Yuan and M. Su, "A fully decentralized control of grid-connected cascaded inverters," *IEEE Trans. Sustainable Energy*, vol. 10, no. 1, pp. 315-317, Jan. 2019.

[2] N. Pogaku, M. Prodanovic, and T. C. Green, "Modeling, analysis and testing of autonomous operation of an inverter-based microgrid," *IEEE Trans. Power Electron.,* vol.22, no.2, pp.613-625, Mar.2007.

[3] J. C. Vasquez, J. M. Guerrero, and A. Luna, "Adaptive droop control applied to voltage-source inverters operating in grid-connected and islanded modes," IEEE Trans. Ind. Electron., vol.56, no.10, pp.4088-4096, Oct.2009.

[4] Z. Liu, M. Su, Y. Sun, L. Li, H. Han, X. Zhang, M. Zheng."Optimal criterion and global/sub-optimal control schemes of decentralized economical dispatch for AC microgrid," *International Journal of Electrical Power & Energy Systems*, vol.104, pp.38-42, Jan. 2019.

[5] M. C, Chandorkar, D. M. Divan, and R. Adapa, "Control of parallel connected inverters in standalone ac supply systems," *IEEE Trans. Ind. Appl.,* vol.29, no.1 pp.136-143, Jan.1993.

[6] J. Rocabert, A. Luna, F. Blaabjerg, and P. Rodriguez, "Control of power converters in AC microgrids," *IEEE Trans. Power Electron.,* vol.27, no.11, pp.4734-4739, Nov.2012.

[7] K. Debrabandere, B. Bolsens, J. Van den Keybus, A. Woyte, J. Driesen, and R. Belmans, "A voltage and frequency droop control method for parallel inverters," *IEEE Trans. Power Electron.,* vol.22, no.4, pp.1107-1115, Jul.2007.

[8] H. Alrajhi Alsiraji and R. El-Shatshat, "Comprehensive assessment of virtual synchronous machine based voltage source converter controllers," *IET Generation, Transmission & Distribution*, vol. 11, no. 7, pp. 1762-1769, May 2017.

[9] J. Liu, Y. Miura, H. Bevrani and T. Ise, "Enhanced Virtual Synchronous Generator Control for Parallel Inverters in Microgrids," *IEEE Transactions on Smart Grid*, vol. 8, no. 5, pp. 2268-2277, Sep. 2017.

[10] W. S. Im, C. Wang, W. Liu, L. Liu and J. M. Kim, "Distributed virtual inertia based control of multiple photovoltaic systems in autonomous microgrid," *IEEE/CAA Journal of Automatica Sinica*, vol. 4, no. 3, pp. 512-519, Jul. 2017.

[11] S. Mishra, D. Pullaguram, S. Achary Buragappu and D. Ramasubramanian, "Single-phase synchronverter for a grid-connected roof top photovoltaic system," *IET Renewable Power Generation*, vol. 10, no. 8, pp. 1187-1194, Sep. 2016.

[12] Y. Ma, W. Cao, L. Yang, F. Wang and L. M. Tolbert, "Virtual Synchronous Generator Control of Full Converter Wind Turbines With Short-Term Energy Storage," *IEEE Transactions on Industrial Electronics*, vol. 64, no. 11, pp. 8821-8831, Nov. 2017.

[13] Y. Fu, Y. Wang and X. Zhang, "Integrated wind turbine controller with virtual inertia and primary frequency responses for grid dynamic frequency support," *IET Renewable Power Generation*, vol. 11, no. 8, pp. 1129-1137, Jun. 2017.

[14] H.-P. Beck and R. Hesse, "Virtual synchronous machine," in *Proc. 9th Int. Conf. Elect. Power Quality Utilisation*, Barcelona, Spain, Oct. 2007.

[15] Y. Hirase, K. Sugimoto, K. Sakimoto and T. Ise, "Analysis of Resonance in Microgrids and Effects of System Frequency Stabilization Using a Virtual Synchronous Generator," *IEEE Journal of Emerging and Selected Topics in Power Electronics*, vol. 4, no. 4, pp. 1287-1298, Dec. 2016.

[16] T. Kerdphol, F. S. Rahman, Y. Mitani, M. Watanabe and S. Küfeoğlu, "Robust Virtual Inertia Control of an Islanded Microgrid Considering High Penetration of Renewable Energy," *IEEE Access*, vol. 6, pp. 625-636, Jun. 2018.

[17] I. Serban, and C. P. Ion, "Microgrid control based on a grid-forming inverter operating as virtual synchronous generator with enhanced dynamic response capability," *International Journal of Electrical Power & Energy Systems*, vol. 89, pp. 94-105, Jul. 2017.

[18] B. Li, L. Zhou, X. Yu, C. Zheng and J. Liu, "Improved power decoupling control strategy based on virtual synchronous generator," *IET Power Electronics*, vol. 10, no. 4, pp. 462-470, Mar. 2017.

[19] Qing-Chang Zhong and G. Weiss, "Synchronverters: inverters that mimic synchronous generators," *IEEE Trans. Ind. Electron.*, vol. 58, no. 4, pp. 1259-1267, Apr. 2011.

[20] Z. Shuai, Y. Hu, Y. Peng, C. Tu and Z. J. Shen, "Dynamic Stability Analysis of Synchronverter-Dominated Microgrid Based on Bifurcation Theory," *IEEE Transactions on Industrial Electronics*, vol. 64, no. 9, pp. 7467-7477, Sep. 2017.

[21] S. Dong and Y. C. Chen, "Adjusting Synchronverter Dynamic Response Speed via Damping Correction Loop," *IEEE Transactions on Energy Conversion*, vol. 32, no. 2, pp. 608-619, Jun. 2017.

[22] V. Natarajan and G. Weiss, "Synchronverters With Better Stability Due to Virtual Inductors, Virtual Capacitors, and Anti-Windup," *IEEE Trans. Industrial Electronics*, vol. 64, no. 7, pp. 5994-6004, Jul. 2017.

[23] M. Dreidy, H. Mokhlis, and S. Mekhilef, " Inertia response and frequency control techniques for renewable energy sources: A review," *Renewable and Sustainable Energy Reviews*, vol. 69, pp. 144-155, Mar. 2017.

[24] H. Bevrani, T. Ise, and Y. Miura, "Virtual synchronous generators: A survey and new perspectives,"*International Journal of Electrical Power & Energy Systems*," vol. 54, pp. 244-254, Jan. 2014.

[25] M. A. Torres L., L. A. C. Lopes, L. A. Morán T. and J. R. Espinoza C., "Self-Tuning Virtual Synchronous Machine: A Control Strategy for Energy Storage Systems to Support Dynamic Frequency Control," *IEEE Trans. Energy Conversion*, vol. 29, no. 4, pp. 833-840, Dec. 2014.

[26] J. Alipoor, Y. Miura, and T. Ise, "Power system stabilization using virtual synchronous generator with alternating moment of inertia," *IEEE J. Emerg. Sel. Topics Power Electron.*, vol. 3, no. 2, pp. 451-458, Jun. 2015.

[27] N. Soni, S. Doolla, and M. C. Chandorkar, "Improvement of transient response in microgrids using virtual inertia," *IEEE Trans. Power Del.*, vol. 28, no. 3, pp. 1830-1838, Jul. 2013.

[28] C. Andalib-Bin-Karim, X. Liang and H. Zhang, "Fuzzy-Secondary-Controller-Based Virtual Synchronous Generator Control Scheme for Interfacing Inverters of Renewable Distributed Generation in Microgrids," *IEEE Transactions on Industry Applications*, vol. 54, no. 2, pp. 1047-1061, Mar.-Apr. 2018.

[29] J. Fang, H. Li, Y. Tang and F. Blaabjerg, "Distributed Power System Virtual Inertia Implemented by Grid-Connected Power Converters," *IEEE Trans. Power Electron.*, vol. 33, no. 10, pp. 8488-8499, Oct. 2018.

[30] J. Fang, H. Li, Y. Tang and F. Blaabjerg, "On the Inertia of Future More-Electronics Power Systems," *IEEE J. Emerg. Sel. Topics Power Electron.,* 2018. Doi: 10.1109/JESTPE.2018.2877766.

[31] J. Fang, R. Zhang, H. Li and Y. Tang, "Frequency Derivative-based Inertia Enhancement by Grid-Connected Power Converters with a Frequency-Locked-Loop," *IEEE Trans. Smart Grid*, 2018. Doi: 10.1109/TSG.2018.2871085.

[32] X. Hou, H. Han, C. Zhong, W. Yuan, M. Yi and Y. Chen, "Improvement of transient stability in inverter-based AC microgrid via adaptive virtual inertia," *2016 IEEE Energy Conversion Congress and Exposition (ECCE)*, Milwaukee, WI, 18-22 Sep.2016, pp. 1-6.

[33] A. Isidori. *Nonlinear control systems*. Springer Science & Business Media, 2013.

[34] J. Liu, Y. Miura, and T. Ise, " Comparison of dynamic characteristics between virtual synchronous generator and droop control in inverter-based distributed generators," *IEEE Trans. Power Electron.,* vol.31, no.5, pp.3600-3611, May 2016.

[35] Y. Sun, X. Hou, J. Yang, H. Han, M. Su, and J. M. Guerrero, "New perspectives on droop control in AC microgrid," *IEEE Transactions on Ind. Electron.*, vol. 64, no. 7, pp. 5741-5745, Jul. 2017.

[36] J. He and Y. W. Li, "Analysis, Design, and Implementation of Virtual Impedance for Power Electronics Interfaced Distributed Generation," *IEEE Trans. Industry Applications*, vol. 47, no. 6, pp. 2525-2538, Nov.-Dec. 2011.

[37] H. Zhang, S. Kim, Q. Sun and J. Zhou, "Distributed Adaptive Virtual Impedance Control for Accurate Reactive Power Sharing Based on Consensus Control in Microgrids," *IEEE Transactions on Smart Grid*, vol. 8, no. 4, pp. 1749-1761, July 2017.

[38] J. Machowski, J. W. Bialek, and J. R. Bumby, *Power System Dynamics: Stability and Control, 2nd ed*. Chippenham, Wiltshire, UK: Wiley, 2008.

[39] X. Hou, Y. Sun, X. Zhang, G. Zhang, J. Lu and F. Blaabjerg, "A Self-Synchronized Decentralized Control for Series-Connected H-Bridge Rectifiers," *IEEE Trans. Power Electronics*, vol. 34, no. 8, pp. 7136-7142, Aug. 2019.

[40] W. Wang and J. J. E. Slotine, "On partial contraction analysis for coupled nonlinear oscillators," *Biological cybernetics*, vol.92, no.1, pp.38-53, Dec.2004.

[41] M. Sinha, F. Dorfler, B.B. Johnson, and S.V. Dhople, "Uncovering

droop control laws embedded within the nonlinear dynamics of Van der Pol Oscillators," *IEEE Trans. Control of Network Systems*, vol. 4, no. 2, pp. 347-358, June 2017.

[42] J. W. Simpson-Porco, Q. Shafiee, F. Dorfler, J. C. Vasquez, J. M. Guerrero, and F. Bullo, "Secondary frequency and voltage control of islanded microgrids via distributed averaging," *IEEE Trans. Ind. Electron.,* vol.61, no.11, pp.7025-7038, Nov.2015.

[43] W. Ren, R. W. Beard, and E. M. Atkins, "Information consensus in multivehicle cooperative control: Collective group behavior through local interaction," *IEEE Control Syst. Mag.*, vol. 27, no. 2, pp. 71–82, 2007.

[44] R. Olfati-Saber, J. A. Fax, and R. M. Murray, "Consensus and cooperation in networked multi-agent systems," *Proc. IEEE*, vol. 95, no. 1, pp. 215–233, 2007.

[45] L. Lin-Yu and C. Chia-Chi, "Consensus-based secondary frequency and voltage droop control of virtual synchronous generators for isolated AC micro-grids," *IEEE Journal on Emerging and Selected Topics in Circuits and Systems*, vol.5, no.3, pp.443-455, Sep.2015.

[46] P. M. Anderson and A. A. Fouad. *Power system control and stability*. John Wiley & Sons, 2008, ch. 2, pp. 13–17.

[47] K. Ledoux, P. W. Visser, J. D. Hulin and H. Nguyen, "Starting Large Synchronous Motors in Weak Power Systems," *IEEE Trans. Industry Applications*, vol. 51, no. 3, pp. 2676-2682, May-Jun. 2015.

[48] Y. A. I. Mohamed and E. F. El-Saadany, "Adaptive Decentralized Droop Controller to Preserve Power Sharing Stability of Paralleled Inverters in Distributed Generation Microgrids," *IEEE Transactions on Power Electronics*, vol. 23, no. 6, pp. 2806-2816, Nov. 2008.

**Xiaochao Hou** (S'16) received the B.S. and M.S. degrees from the School of Information Science and Engineering, Central South University, Changsha, China, in 2014 and 2017, respectively, where he is currently working toward Ph.D. degree in power electronics and power transmission. Now he is a joint Ph.D. student supported by the China Scholarship Council with the School of Electrical and Electronic Engineering of Nanyang Technological University. His research interests include distributed micro-grid, and power-electronic enabled power network.

**Yao Sun** (M'14) received the B.S., M.S. and Ph.D. degrees from the School of Information Science and Engineering, Central South University, Changsha, China, in 2004, 2007 and 2010, respectively. He is currently with the School of Information Science and Engineering, Central South University, China, as a professor. His research interests include matrix converter, micro-grid and wind energy conversion system.
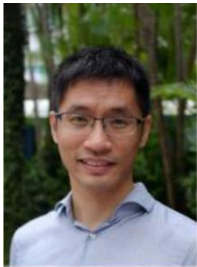
**Xin Zhang** (M'15) received the Ph.D. degree in Automatic Control and Systems Engineering from the University of Sheffield, U.K., in 2016 and the Ph.D. degree in Electronic and Electrical Engineering from Nanjing University of Aeronautics & Astronautics, China, in 2014. Currently, he is an Assistant Professor of Power Engineering at the School of Electrical and Electronic Engineering of Nanyang Technological University. He was the Postdoctoral Research Fellow (2017.01 - 2017.09) at the City University of Hong Kong and the Research Associate (2014.02 - 2016.12) at the University of Sheffield. He is generally interested in power electronics, power system, and advanced control theory, together with their applications in various sectors.

**Jinghang Lu** (S'14-M'18) received the B.Sc. degree in electrical engineering from Harbin Institute of Technology, China, in 2009, two M.Sc. degrees both in electrical engineering from Harbin Institute of Technology, China, in 2011, and University of Alberta, Canada, in 2014, respectively, and the Ph.D. degree in Power Electronics from Aalborg University, Aalborg, Denmark, in 2018. From 2018 to 2019, he was a Research Fellow with Nanyang Technological University, Singapore. He is currently an Assistant Professor with Harbin Institute of Technology (Shenzhen), Shenzhen, China. His research interests include uninterruptible power supply, microgrid, and control of power converters.

**Peng Wang** (F'18) received the B.Sc. degree in electronic engineering from Xi'an Jiaotong University, Xi'an, China, in 1978, the M.Sc. degree from Taiyuan University of Technology, Taiyuan, China, in 1987, and the M.Sc. and Ph.D. degrees in electrical engineering from the University of Saskatchewan, Saskatoon, SK, Canada, in 1995 and 1998, respectively. Currently, he is a Professor with the School of Electrical and Electronic Engineering at Nanyang Technological University, Singapore.

**Josep M. Guerrero** (M'04-SM'08-F'15) received the B.S. degree in telecommunications engineering, the M.S. degree in electronics engineering, and the Ph.D. degree in power electronics from the Technical University of Catalonia, Barcelona, in 1997, 2000 and 2003, respectively.

Since 2011, he has been a Full Professor with the Department of Energy Technology, Aalborg University, Denmark, where he is responsible for the Microgrid Research Program. His research interests is oriented to different microgrid aspects, including power electronics, distributed energy-storage systems, hierarchical and cooperative control, energy management systems.